Integrated proteomics and metabolomics analysis reveals new insight into the synergistic antitumor effect of valproic acid plus simvastatin in prostate cancer xenograft model associated with downmodulation of YAP/TAZ signaling

Federica Iannelli
Experimental Pharmacology, Istituto Nazionale Tumori —IRCCS— Fondazione G. Pascale, 80131 Naples, Italy
Rita Lombardi
Sperimentazione Animale, Istituto Nazionale Tumori—IRCCS—Fondazione G. Pascale, 80131 Naples, Italy
Susan Costantini
Experimental Pharmacology, Istituto Nazionale Tumori —IRCCS— Fondazione G. Pascale, 80131 Naples, Italy
Maria Serena Roca
Experimental Pharmacology, Istituto Nazionale Tumori —IRCCS— Fondazione G. Pascale, 80131 Naples, Italy
Laura Addi
Experimental Pharmacology, Istituto Nazionale Tumori —IRCCS— Fondazione G. Pascale, 80131 Naples, Italy
Francesca Bruzzese
Sperimentazione Animale, Istituto Nazionale Tumori—IRCCS—Fondazione G. Pascale, 80131 Naples, Italy
Elena Di Gennaro
Experimental Pharmacology, Istituto Nazionale Tumori —IRCCS— Fondazione G. Pascale, 80131 Naples, Italy
Alfredo Budillon
a.budillon@istitutotumori.na.it

Scientific Directorate, Istituto Nazionale Tumori—IRCCS—Fondazione G. Pascale, 80131 Napoli, Italy
Biagio Pucci
Experimental Pharmacology, Istituto Nazionale Tumori —IRCCS— Fondazione G. Pascale, 80131 Naples, Italy

Research Article

Keywords: Drug-repurposing, Valproic Acid, Simvastatin, proteomics, metabolomics, Prostate Cancer

Posted Date: March 15th, 2024

DOI: https://doi.org/10.21203/rs.3.rs-4086640/v1

Additional Declarations: No competing interests reported.

Abstract

Background: Despite advancements in therapeutic approaches, including taxane-based chemotherapy and androgen receptor targeting agents, metastatic castration-resistant prostate cancer (mCRPC) remains an incurable tumour, underlying the need of novel strategies that can target the complexities of this disease and bypass the development of drug-resistance mechanisms. We previously demonstrated the synergistic antitumor interaction of the antiepileptic with histone deacetylase inhibitory activity valproic acid (VPA), and the lipid-lowering drug simvastatin (SIM). This combination sensitizes mCRPC cells to docetaxel treatment, both *in vitro* and *in vivo* models, by targeting cancer stem cells compartment via mevalonate pathway/YAP axis modulation.

Methods Here, by a combined proteomic and metabolomic/lipidomic approach we characterized tumor samples derived from 22Rv1 mCRPC cells xenografted mice, treated or not with VPA/SIM combination, coupled with an in deep bioinformatics analysis.

Results We confirmed a specific impact of VPA/SIM on Hippo-YAP signaling pathway, functionally related with modulation of cancer-related extracellular matrix biology and metabolic reprogramming, providing further insights into the molecular mechanism of the VPA/SIM antitumor effect.

Conclusions In the current study, we present an in-depth exploration of the potential to repurpose in mCRPC treatment two generic and safe drugs, valproic acid (VPA) and simvastatin (SIM), that already showcased anti-tumor efficacy in combination, primarily affecting cancer stem cell compartment via MVP/YAP axis modulation. Bioinformatics analysis of LC-MS/MS proteomics and of 1H-NMR metabolomics/lipidomics results, confirmed a specific impact of VPA/SIM on Hippo-YAP

1. Background

Prostate cancer (PCa) is the second most frequent malignancy in men worldwide (1). Despite the success of androgen deprivation therapy (ADT) in suppressing tumor growth, most patients invariably progress to castration-resistant metastatic prostate cancer (mCRPC) (2). Although several specific therapeutic options have been developed, mCRPC remains a condition with a poor prognosis and a median survival for patients of approximately two to three years (3). Major systemic treatment options for mCRPC patients include taxane-based chemotherapy (docetaxel and cabazitaxel) and androgen receptor target agents such as abiraterone or enzalutamide. Even though the use of these drugs has improved clinical outcomes prolonging the lifespan, many patients develop resistance (4). Thus novel combination treatment strategies are needed to target signaling pathways involved in mCRPC progression and drug resistance. In a recent study we suggested the potential to repurpose in mCRPC treatment the antiepileptic agent with histone deacetylases inhibitors (HDACi) activity, valproic acid (VPA), and the lipid-lowering drug simvastatin (SIM), that inhibit HMG-CoA reductase (HMGCR), the first step of the mevalonate pathway (MVP). In details, we demonstrated, for the first time, both *in vitro* and *in vivo* models, the synergistic antitumor interaction between VPA and SIM and the ability of this combination to

sensitize mCRPC cells to docetaxel and to revert docetaxel-resistance. Interestingly, we observed a reciprocal ability of both VPA and SIM to target histone acetylation and HMGCR expression, strengthening our hypothesis of a synergistic interaction of these drugs (5). Moreover, we showed the capacity of VPA/SIM combined approach to target the cancer stem cells (CSCs) compartment via the inhibition of the oncogene Yes-associated protein (YAP), a transcriptional regulator whose hyperactivation is a hallmark of several solid tumors, including PCa, being essential for cancer initiation/growth and drug-resistance (5–7). Mechanistically, we demonstrated that VPA/SIM combination downmodulated YAP oncogene expression and activity through the concurrent modulation of the MVP and of the key cellular metabolic sensor AMP-activated protein kinase (AMPK). In the present study, to further investigate in depth the mechanism of the unique synergistic antitumor interaction between VPA and SIM, we took advantage of liquid chromatography-tandem mass spectrometry (LC-MS/MS)-based shotgun proteomics to analyze tumor tissues obtained by an *in vivo* experiment from our study reported above (5). In details, we analyzed tumor tissues from 22Rv1 PCa cells xenograft model, and identified differentially expressed proteins between untreated and VPA/SIM treated groups. Notably, this approach confirmed a specific impact of VPA/SIM on Hippo-YAP signaling and revealed the ability of this combination treatment to modulate biological processes associated with extracellular matrix (ECM) and metabolic pathways. Likewise, on the same tumor tissues samples we performed metabolomics and lipidomics analysis, by proton Nuclear Magnetic Resonance (^{1}H-NMR) approach, confirming metabolic reprogramming induced by VPA/SIM combined treatment (Additional file 1).

Overall, our study provided new insights into the mechanisms behind the antitumor effect of VPA/SIM combination suggesting that this approach can be extended to other cancer models in order to be combined with standard anticancer therapies.

2. Methods

2.1 Shotgun proteomics on tumor samples

Tumor samples were collected from 22Rv1 xenografted tumors. Briefly, five weeks old female NOD/SCID athymic mice (Charles River, Wilmington, MA, USA) were injected subcutaneously with 22Rv1 cells and randomly assigned to receive VPA/SIM combination (200 mg/Kg and 2 mg/Kg, respectively, i.p. daily for 2 weeks), or their vehicles. This study have been performed in compliance with institutional guidelines and regulations (Directive 2010/63/EU; Italian Legislative Decree DLGS 26/2014) and after approval from the appropriate institutional review board (N.865/2015-PR). Xenografted tumors grew rapidly and reached the endpoint size within 3 weeks; at this time-point VPA/SIM combination produced a significant tumor growth inhibition compared with control mice and tumors from each treatment group were collected (5). For proteomic analysis, tumor samples were lysed with 0.2% RapiGest SF (Waters, MA, USA) in 50 mM ammonium bicarbonate using the Tissue Lyser II system (Qiagen, Hilden, Germany). After samples centrifugation for 30 min at 14,000 rmp at 4˚C, the supernatants were lysed in ice for 2 hours, denatured at 80˚C for 15 min and then sonicated.. The amount of proteins was evaluated by Bradford

assay. 20 µg of total proteins, were reduced by 10 mM dithiothreitol and then alkylated by 24 mM iodoacetamide, both stages at 37˚C for 1 hour (Sigma Aldrich, Merck KGaA, Germany). Afterwards, in solution protein digestion was performed using trypsin at a 1:50 ratio w/w (Promega Corporation, Madison, WI, USA). Samples were desalting by stage Tip C18 (Millipore, Merck KGaA, Munich, Germany) and dried in vacuum system. About 5 µg of peptides were resuspended in 0.1% TFA and injected into Dionex UltiMate 3000 nano system (Thermo Fischer Scientific, CA, USA) coupled with an AmaZon ETD mass spectrometer (Bruker Daltonics, Bremen, Germany). Peptide samples were loaded onto a Pepmap precolumn (2 cm × 100 µm, 5 µm), followed by separation on 25 cm Nano column (0.075 µm, Acclaim PepMap100, C18, Thermo Fischer Scientific, CA, USA), at a flow rate of 300 nL/min. Multistep 360-min gradients of ACN were used. The mass spectrometer equipped with nanoBoosterCaptiveSpray™ ESI source was operated in data-dependent-acquisition mode. For MS generation, enhanced resolution and a trap ICC value of 400 000 were used; for MS/MS acquisition, the ICC target was increased to 1000000. CID MS/MS fragmentation was set to fragment the ten most abundant MS peaks (Top 20). The obtained chromatograms were elaborated using Compass Data Analysis™ v.4.2 (Bruker Daltonics, Bremen, Germany) and the resulting mass lists were processed using Mascot search engine (v.2.7.0). Database searching was restricted to the human Swissprot database. Trypsin as an enzyme, carbamidomethyl (C) as a fixed modification and oxidation (M) as variable modification were set in search parameters. Mass tolerance for all identifications was generally fixed at 2 Da for the precursor ions and 0.8 Da for the product ions. Data were filtered using a global FDR < 5% and only proteins with at least one unique identical peptide sequence (p-value < 0.05) were considered identified (8).

2.2 Protein quantification analysis

Progenesis QI for proteomics v. 4.2 (Non-linear Dynamics, Newcastle, England) was used as label-free quantification platform. Briefly, raw data were imported and the ion intensity maps of all runs (4 for CTR group and 3 for VPA + SIM group) used for the alignment process Only alignment scores above 60% were accepted. Peak peaking was performed using the default sensitivity and a peak width of 0.15 min and charge states of + 2, +3 + 4 were setting. The survey scan data is used for the quantification of peptide ions without MS/MS data. Data is then normalized to all proteins. Protein identification was achieved using Mascot. Protein abundance was calculated using the sum of all unique peptide normalized ion abundances for that protein on each run (9). To indicate the statistical peptides significance, Anova test p-value ≤ 0.05) and a fold change 2 were applied. Moreover, to afford the multiple testing problem, the FDR adjusted p-values, named q-value, is also provided (q-value ≤ 0.01). Technical variability of each peptide/protein was estimated among replicates from the pooled sample by calculating Pearson correlation coefficients (PCC) using the Perseus (v. 1.6.6.0) (10).

2.3 Immunoblotting

Protein extraction from xenograft tumor samples are described in the proteomic (*see 5.1 paragraph*). About 50 µg of lysates were resolved by SDS-PAGE and performed as previously described (11). Protein extraction of 22Rv1 treated with VPA and/or SIM at the IC_{50}^{96h} doses for 4h or for 24 h. All Western blots were quantified using imageJ software (Rasband, W.S., U.S., National Institutes of Health, Bethesda,

Maryland, USA). Primary antibodies were purchased as follows: Phospho-LATS1 (Thr1079) (D57D3) Rabbit mAb#8654 Cell Signaling Technology (Leiden, Netherlands). Anti-LATS1 antibody (ab70562), Abcam (Cambridge, UK). β-actin C4 (sc-47778) from Santa Cruz Biotechnology Inc., (Dallas, TX, USA). Secondary antibodies were purchased as follows: polyclonal swine anti-rabbit immunoglobulins/horseradish peroxidase (HRP)-linked IgG secondary from Abcam (Cambridge, UK).

2.4 Functional annotation analysis

Gene Ontology (GO) enrichment and pathway analyses were performed using the Database for Annotation, Visualization and Integrated Discovery (DAVID) v6.8 (https://david.ncifcrf.gov/) (12). g:Profiler (version e94_eg41_p11) was performed as follows: GO analyses (GO molecular function (GO: MF), GO cellular component (GO: CC), and GO biological process (GO: BP)) were carried out sequentially. The biological pathways used WikiPathways (WP) databases. (13). The enrichment analysis was performed against Reactome version 66 and the web link is as follows: https://reactome.org/PathwayBrowser. 2.5 Protein network analyses. The networks between MS-identified proteins, whose expression changes, were obtained by (Ingenuity Pathway Analysis) IPA software (GeneGo Inc., St. Joseph, MI, USA) visualizing proteins as hubs and the relationship between proteins as edges.

2.5 Extraction of the polar and lipidic fractions in tumor samples and 1H-NMR metabolomic/lipidic analysis

The tissues (100 mg) related to three untreated and treated groups were subjected to a chemical extraction based on methanol, chloroform and water to separate the polar and lipidic fractions. The lipidic fractions were dissolved in 700 µL of $CDCl_3$, and the polar fractions were dissolved in 630 µL of PBS-D_2O and 70 µL of sodium salt of 3-(trimethylsilyl)-1-propanesulfonic acid (1% in D_2O) used as the internal standard. ^1H spectra on these polar and lipidic fractions were acquired at 300 K by a 600 MHz Bruker spectrometer equipped with a TCI cryoprobe for 256 and 512 scans, respectively.

2.6 Statistical analysis

The statistics of the shotgun proteomics experiment is performed by Progenesis QI for proteomics v. 4.2 and reported in the specific section. Representative results from a single western blot analysis experiment are presented; additional experiments yielded similar results.

All NMR spectral regions were bucketed by AMIX package (Bruker, Biospin GmbH, Rheinstetten, Germany) and normalized to the total spectrum area using Pareto scaling. Partial least squares-discriminant analysis (PLS-DA) and Loading plot by Metabo Analyst v5.0 tool (14) were performed to compare the spectra obtained on the untreated and treated samples

3. Results

3.1 Proteomics profiling of prostate xenograft tumor samples

Label-free proteomic analysis was applied in order to identify and quantify proteins whose abundance is significantly different between untreated (CTR) *vs* VPA/SIM treated mouse tumor samples described in Fig. 1A. Taking advantage of Progenesis software, 1030 proteins were quantified using the following filters: fold change ≥ 2 and Anova test p-value ≤ 0.05 (Additional file 2). Among these proteins, 424 were up-regulated and 606 were down-regulated by the VPA/SIM treatment, respectively.

Principal component plot (PCA), derived from unsupervised multivariate analysis of differential protein expression profiles, demonstrated a close correlations between the spot maps of the biological replicates, thus highlighting the experimental reproducibility (Fig. 1B). Furthermore, Pearson correlation coefficients showed a high reproducibility of peptides/proteins levels among control biological replicates (CTR_1 *vs* CTR_2) or treated biological replicates (VPA/SIM_1 *vs* VPA/SIM_2). On the other hand, CTR_1 *vs* VPA/SIM_1 analysis showed lower correlation coefficient, accordingly with the reported differential protein expression between the two groups (Fig. 1C).

3.2 Hippo-Yap signalling resulted one of the main enriched pathway modulated by VPA/SIM combination

Signalling pathway enrichment analysis carried out on the 1030 differentially expressed proteins by g:Profiler software, highlighted, among others, epigenetic and histone modification, thus confirming VPA activity on tumor cells, as well as AR signalling, extracellular matrix and cytoskeleton targeting, and metabolic pathways engagement (Fig. 2A). Remarkably, also Hippo-YAP signalling emerged as one of the main enriched pathway modulated by VPA/SIM treatment, thus confirming our previous results (5). In detail, as reported by the normalized abundance calculated by peptide ion signal peaks intensity, we found a clear down regulation of YAP and its targets CTGF, CycD1 and ANKH1 in VPA/SIM *vs* CTR groups (Fig. 2B). Interestingly, we also found the downregulation of TEA domain (TEAD), a transcription factor that directly mediates YAP-induced gene expression, along with the upregulation of the 14-3-3, a protein responsible for YAP cytoplasmic retention and degradation following its phosphorylation in Serine 127 (Fig. 2B). On the other hand, in VPA/SIM-treated tumor samples we also found the up-regulation of YAP up-stream negative regulators such as LATS1 and AMPK (Fig. 2C). LATS1 represents the last effector of the Hippo-YAP pathway that, recruited upon its phosphorylation in tyrosine 1097, inactivates YAP. Thus, we investigated LATS1 expression and phosphorylation in tyrosine 1097 in tumor lysates treated with VPA/SIM combination by western blot, confirming both increased expression and 1097-phosphorylation (Fig. 2D).

3.3 New molecular mechanism of VPA/SIM combination associated with ECM reorganization

Next, functional annotation analyses were performed to establish the biological processes associated with the 1030 differentially expressed proteins by Gene Ontology (GO) enrichment analysis, using DAVID software (Fig. 3). The most relevant enriched GO terms are reported in Fig. 3A. Among twenty-one GO biological processes selected, eight were associated with cell architecture and cytoskeleton organization, including “regulation of cell junction assembly” and “actin filament reorganization” as the two top process selected, as well as the extracellular matrix (ECM) organization and disassembly, consistently with enriched pathway analysis reported above. Notably, several proteins within these last biological processes, such as Calpain-2 catalytic subunit (CAN2), Calpain-1 catalytic subunit (CAN1), Calpain small subunit (CPNS1), Elastin (ELN), Matrix metalloproteinase 1 (MMP1), Matrix metalloproteinase 10 (MMP10), Laminin subunit gamma-1 (LAMC1), Periostin (POSTN), Ras-related protein Rab-11A (RB11A), Microtubule-associated protein 2 (MTAP2), Protein-tyrosine phosphatase mu (PTPRM) and Serine/threonine-protein kinase Unc-51-like kinase 1 (ULK1), were reduced in VPA/SIM treated tumor samples (Table 1). Of note, these proteins, beyond their structural roles, are involved in several pathways influencing tumor growth and progression (15–23).

Table 1. List of proteins involved in the two interesting biological processes: “Cell architecture and cytoskeleton organization” and “Biological Metabolic Process”.

Biological Process	Gene names	Protein names	UniProt Accession numbers	Fold- change VPA+SIM/CTR
Cell architecture and cytoskeleton organization	CAN2	Calpain-2 catalytic subunit	P17655	-3.58
	CAN1	Calpain-1 catalytic subunit	P07384	-7.74
	CPNS1	Calpain small subunit	P04632	-2.40
	ELN	Elastin	P15502	-3.90
	MMP1	Matrix metalloproteinase 1	P03956	-5.06
	MMP10	Matrix metalloproteinase 10	P09238	-2.12
	LAMC1	Laminin subunit gamma-1	P11047	-4.75
	POSTN	Periostin	Q15063	-2.73
	RB11A	Ras-related protein Rab-11A	P62491	-4.16
	MTAP2	Microtubule-associated protein 2	P11137	-4.14
	PTPRM	Protein-tyrosine phosphatase mu	P28827	-8.60
	ULK1	Serine/threonine-protein kinase ULK1	O75385	-42.92
Biological Metabolic Process	HCD2	3-hydroxyacyl-CoA dehydrogenase type-2	Q99714	+2.01
	ECHD2	Enoyl-CoA hydratase	Q86YB7	-2.92
	MDH1	Malate dehydrogenase, cytoplasmic	P40925	+2.33
	MDH2	Malate dehydrogenase, mitochondrial	P40926	+7.03
	SDHA	Succinate dehydrogenase, mitochondrial	P31040	+6.93
	ACON	Aconitate hydratase, mitochondrial	Q99798	+3.32
	CISY	Citrate synthase, mitochondrial	O75390	-2.84

ENOA	Alpha-enolase	P06733	+2.88
ALDOA	Fructose-bisphosphate aldolase A	P04075	+2.89
ASGL1	Isoaspartyl peptidase/L-asparaginase	Q7L266	-2.67
G6PI	Glucose-6-phosphate isomerase	P06744	+3.44

For each protein we reported gene and protein names, accession numbers by Uniprot database and fold changes obtained comparing the mean normalized peptide ion signal peak intensities in the 22Rv1 VPA/SIM treated vs CTR groups.

3.4 ECM related proteins are directly associated with YAP in one main network

Interestingly, it was demonstrated that increased ECM stiffness promotes cell spreading, the nuclear localization of YAP and the up-regulation of its target genes (24). Thus, we hypothesized that ECM remodelling and YAP modulation induced by VPA/SIM combination, could be functionally related. In order to address this hypothesis we interrogated the Ingenuity Pathway Analysis (IPA), revealing, by looking for direct interaction, that 11 out of 12 identified proteins, closely cluster together and with YAP. In detail, we found that “Metastasis of cells”, “Morphology of malignant tumor”, “Proliferation of stem cells, mesenchymal stem cells and connective tissue cells”, “Differentiation of tumor cells”, “Angiogenesis”, “Migration of tumor cell lines, prostate cancer cell lines and carcinoma cell lines” and “Invasion of tumor cell lines” were the IPA-predicted top molecular and cellular functions (Fig. 4).

3.5 VPA/SIM combination induced dysregulation of metabolism process

After cell architecture/cytoskeleton and ECM organization processes, the most represented biological processes highlighted by both functional and GO enrichment analysis resulted related with metabolic pathways (Fig. 2A and 3A).

An additional in depth analysis investigating Kyoto Encyclopedia of Genes and Genomes (KEGG) pathways, also confirmed in the top list a number of metabolismassociated pathways involved in the differential protein expression profiles between untreated and VPA/SIM-treated tumor tissues samples (Fig. 3B).

Among the proteins involved in the metabolic processes, we identified Enoyl-CoA hydratase (ECHD2) and 3-hydroxyacyl-CoA dehydrogenase type-2 (HCD2) that are down- and up-regulated in the VPA/SIM treated group, respectively, catalyzing the second and the third step in the beta-oxidation pathway of fatty acid metabolism (Table 1).

Moreover, among the most representative biological metabolic processes modulated by VPA/SIM is the tricarboxyloic acid cycle (TCA). In detail, in VPA/SIM treated tumors we observed an increased expression of mitochondrial aconitase (ACON) (Table 1), that catalyzes the interconversion of citrate to isocitrate in the second step of the TCA cycle (25) (Fig. 6). Conversely, we found a lower expression of citrate synthase (CISY), a rate-limiting enzyme in the citrate cycle that is capable to catalyze oxaloacetate and acetyl-CoA to citrate. Furthemore, we found both cytosolic and mitochondrial malate dehydrogenases (MDH1 and MDH2, respectively), upregulated in the VPA/SIM treated group. Finally, also mitochondrial succinate dehydrogenase (SDHA) with the unique property to participate in both the citric acid cycle and the electron transport chain, is up-regulated by the treatment. This enzyme is embedded in the inner mitochondrial membrane performing the chemical reaction that produce fumarate from succinate.

The Voronoi diagram visualization by Reactome analysis, confirmed that several pathways are grouped according to the relationships “in metabolism pathway” including “metabolism of lipid pathway” as a contiguous region (Additional file 3) (26).

3.6 VPA/SIM combination influenced the metabolomics and lipidomics profiling

To confirm the impact of the modulated enzymes indicated above, next, taking advantage of ^{1}H-NMR spectroscopy, we evaluated the metabolomics/lipidomics profiling on the same tissue samples from untreated and VPA/SIM treated tumors. As reported in Fig. 5A, multivariate statistical analysis evidenced a marked difference between treated and control samples, with a total variance equal to 59.2%. The Loading plot reported in Fig. 5B showed a significant modulation of several metabolites such as amino acids, intermediates of TCA, urea cycles and glycolysis. Specifically, the levels of citrate, sarcosine, ATP, malate, glucose, aspartate, and citrulline decreased whereas only those of ornithine increased after VPA/SIM treatment (Fig. 5B).

Interestingly, the lower levels of citrate correlated with the lower levels of CISY as well as with the higher levels of ACON reported above, as also suggested elsewhere (27). On the other hand, the lower levels of malate correlated with the higher levels of malate dehydrogenases (MDHs) we found in the VPA/SIM treated group (Table 1). The decrease of glucose levels could be related with the VPA/SIM-induced expression levels of three enzymes (ALDOA, ENOA and G6PI) involved in glycolysis (Table 1). The parallel clear reduction of ATP, also indicated alteration of energy-related pathways. The lower levels of aspartate and the parallel VPA/SIM-induced reduction of asparaginase (ASGL1), might both also contributed to the alteration of TCA cycle. Aspartate also contributed to urea cycle where both ornithine and citrulline are involved. In particular, ornithine is a precursor of citrulline being involved the production of urea from ammonia (urea cycle), and is synthesized itself in the last step of the urea cycle, catalyzed by arginase that cleaves arginine to produce urea and ornithine.

Overall, the data related to both metabolomics and proteomics analyses confirmed that VPA/SIM treatment might induced metabolic reprogramming/alterations as summarized in Fig. 6 by a schematic representation.

On the other hand, multivariate statistical analysis of NMR spectra obtained on lipid fractions also evidenced a marked difference between treated *vs* control samples with a total variance equal to 88.1% (Fig. 5C). The loading plot showed that the several proton signals of cholesterol, and fatty acids decreased after treatment (Fig. 5D). These results are in agreement with the reduction of cholesterol levels we have observed in PCa xenograft tumor samples upon VPA/SIM combination treatment (5) and also correlated with data reported above. Indeed, both ACON modulation and citrated reduction have an impact on both cholesterol and fatty acid synthesis (28, 29), Moreover, the decreased levels of fatty acids can be also correlated to an increase of fatty acid degradation following beta-oxidation, a pathway where it is involved the enzyme HCD2 (30), increased by VPA/SIM treatment, as shown by proteomics approach.

4. Discussion

The integration of multi-omics data plays a pivotal role in elucidation of the molecular mechanism of tumorigenesis, new biomarkers discovery and drug targets (31). In the present study, we took advantage of proteomics and metabolomics approach to further investigate the mechanism of the potent antitumor effect exerted by the combination of the two well-known generic drugs VPA and SIM in different prostate tumor cellular models, being also able to sensitize tumor cells to docetaxel and to revert docetaxel-resistance (5). We analyzed tumor tissues from treated and untreated xenograft mouse models, in order to highlight important physiological processes that are normally lacking *in vitro* models such as angiogenesis, stromal interaction influencing tumor growth and metastasis.

One of the most interesting finding of the present study is the confirmation that VPA/SIM synergistic effect involved the modulation of the Hippo signaling pathway, a major player in stem cells and cancer biology with its effectors YAP and the highly related other transcriptional regulator TAZ (transcriptional coactivator with PDZ-binding motif) (32).

Interestingly, YAP, that we confirmed to be downmodulated at the protein level by VPA/SIM treatment as previously shown (5), is recognized as a clinical marker for PCa progression and regulator of mCRPC and correlate with patients' Gleason score, prostate-specific antigen (PSA) levels and extraprostatic extensions, associated with bad prognosis (7). When the Hippo pathway is activated, mammalian MST1/2 phosphorylates and activates LATS1/2, which in turn phosphorylates YAP/TAZ on tyrosine or serine residues inducing YAP/TAZ cytoplasmic retention and inactivation.

Of note, we added additional insight to the mechanism studied in the previous work, demonstrating the VPA/SIM-induced up-regulation of both protein expression and activity of LATS1 in tumor tissue samples. The oncogenic role of YAP/TAZ mainly depends on their nuclear localization, where YAP/TAZ interact with TEAD, that we found downregulated upon treatment, to form a complex that promote the expression and activation of downstream target genes (7). Moreover, the protein 14-3-3 that we found upregulated upon treatment inactivates the proliferative function of phospho-YAP/TAZ by binding and sequestering them in the cytosol, thus preventing their interaction with TEAD transcription factors (33). Furthemore,

Ras-related protein Rab11A, downmodulated by VPA/SIM, is reported to induce YAP protein and inhibit Hippo signalling, thus influencing the cell cycle proteins expression and cell proliferation (23).

In our previous study we focused on the critical relationship between YAP and MVP, rely mainly on CSC behavior and generation in PCa models, showing that VPA/SIM combination was able to downregulate all the principal YAP transcriptional targets, highly enriched in patients with PCa tumors, such as CTGF, CYR61, BIRC5 and ANKH1 (5). Interestingly, in our proteomics study, we confirmed, beyond YAP and TEAD1, also the downregulation of YAP targets such as CTGF, CycD1 and ANKH1 in the VPA/SIM tumor xenograft samples compared to untreated group.

In line with our results, several studies suggested a modulation of YAP phosphorylation, localization, and activity by statins, but most of them reported this effect as independent of MST1/2 and LATS1/2 activity (34, 35). Only few papers described a significant induction of the LATS1 expression upon statins treatment in breast cancer models (36, 37).

In addition, through the proteomic approach and bioinformatics tools, we added new insight to the molecular mechanism of VPA/SIM combination treatment. Indeed, using Gene Ontology analysis related to the Biological Process, we identified a substantial group of proteins related to the ECM Organization. ECM represents one promising avenue of research in cancer therapy being a critical part of the tumor microenvironment, including tumor and stromal cells, vasculature, and non-cellular components that make up a tumor. It is also essential for the construction of the metastatic niche, the microenvironment that tumor cells generate in collaboration with stromal cells when colonizing different sites (38). Interestingly, we observed VPA/SIM-mediated downregulation of calpains (CAN1, CAN2 and CPNS1), whose expression is usually increased in cancer cells, where they can regulate activation of MMPs for ECM remodelling angiogenesis, cancer invasion and metastasis (15, 39).

CPNS1 has been also found up-regulated in docetaxel-resistant mCRPC cell sublines compared with their parental cell lines (40). Moreover, it has been demonstrated that CAN2 can cleave and remove the ligand-binding domain (LBD) from AR, producing a constitutively active form of AR, contributing to PCa cells aggressiveness (15). Similarly, overexpression of MMP-1, that we reported down-regulated by VPA/SIM, was described in PCa compared to benign prostatic hypertrophy (17). Moreover, overexpression of POSTN, also decreased by VPA/SIM, has been associated with worse baseline clinical features, shorter disease-free survival (DFS), and reduced overall survival (OS) in PCa (21). Among those differentially expressed proteins down-regulated by VPA/SIM co-treatment, we also identified MTAP2, another protein of interest in PCa identified as a prognostic marker in several cancers and linked to taxane-based therapies resistance (41). Finally, the Serine/threonine-protein kinase ULK, also downmodulated by VPA/SIM is involved in AR-regulated signalling cascade that promote the autophagic flux in PCa cell proliferation and survival (42).

Alterations of the mechanical properties of the ECM, represented mainly by stiffness and elasticity, can be induced by cancer cells themselves or by stromal cells and represent mechanical inputs that profoundly affect crucial biological aspects of tumor development, such as cell proliferation, differentiation and

apoptosis (43). Similarly, within cancer cells the cytoskeleton needs to be continually reorganized to regulated cell shape and movement, to invade the surrounding tissue, extravasate and reach the metastatic site. Accumulating evidences demonstrated that YAP/TAZ are primary sensors of the cell's physical nature, as defined by cell structure, shape and polarity (44). YAP and TAZ also maintain plasticity in cell–ECM adhesion by limiting the maturation of focal adhesions, enabling cell migration (45). In line with to the above observations, we found that the identified ECM proteins are associated in one main IPA network and all are related to YAP. These results suggested that the VPA/SIM combination influenced ECM reorganization through YAP in our PCa xenograft tumor samples promoting an unfavorable environment for PCa progression. IPA analysis also showed that transforming growth factor-beta (TGF-β) and p53 emerged as main hubs in the network. TGF-β in cooperation with YAP/TAZ plays pivotal roles in the production of fibrogenic factors and ECM proteins which are likely to contribute to cancer progression (46-48). Indeed, it has been demonstrated that YAP and TAZ-deficient fibroblasts are less reactive to TGF-β stimulation *in vitro*, producing less ECM proteins (43). Moreover, POSTN, one of the VPA/SIM down-modulated proteins is an important mediator of TGF-β-induced EMT and metastatic progression in PCa (49). On the other hand, it was reported that missense mutant p53 trigger unscheduled activation of YAP/TAZ in both cancer cells and human primary tumors (44) .

Statins may impair tumor metastatic process by inhibiting cell migration, attachment to the ECM and invasion of the basal membrane as well as angiogenesis, by downregulating MMPs and pro-angiogenic factors (50, 51). More specifically, SIM can inhibit normal actin polymerization and the relative invadopodia formation, decreasing cell motility and spreading in the extracellular matrix contributing to the reduction of metastatic spread (52). Conversely, several studies demonstrated the antimetastatic and anti-angiogenic activities of HDACi, including VPA, in multiple tumors by different mechanisms, including p53 inhibition (53, 54).

We also demonstrated an impact of VPA/SIM co-treatment on PCa xenograft tumor metabolism by identifying several modulated proteins related to metabolic pathways as well as the modulation of several coordinated metabolites. Interestingly, dysregulation of metabolism has been linked with carcinogenesis and the progression of PCa (55). Specific metabolites/enzymes, modulated by VPA/SIM treatment have been directly associated with PCa progression and growth. For example, PCa is associated with fatty acid oxidation abnormality (56) and VPA/SIM downmodulated the fatty acid beta-oxidation enzyme ECHD2, whose expression correlated with the progression, metastasis and drug resistance of PCa, being considered a potential biomarker for PCa diagnosis (57). We also demonstrated an impact of VPA/SIM treatment on TCA cycle whose dysregulation was also reported in PCa. For example decreased expression of CISY, dowmodulated by VPA/SIM, was reported to affect PCa cell proliferation, colony formation, migration, invasion and cell cycle in vitro, and inhibited tumor growth *in vivo* (55). In addition, CISY down-regulation exerted potential inhibitory effects on the lipid metabolism and mitochondrial function of PCa cells (55). Interestingly, decreased CISY activity was found in patients during simvastatin treatment (58). Similar results were obtained in rats in which VPA resulted to be able to decrease CISY (59). Furthermore, germline mutations of SDH gene, whose protein is upregulated by VPA/SIM, have been identified in several types of cancer and have been shown to contribute to an

abnormal accumulation of succinate in the cytosol of tumoral cells and in the extracellular fluids of the patients. These observations suggested that SDHA could be defined as a tumor suppressor and succinate as an oncometabolite capable to promote epithelial-to-mesenchymal transition, angiogenesis stimulation, migration and invasion and amplifying oncogenic cascades (60, 61). We also demonstrated VPA/SIM-mediated downmodulation of asparaginase, an enzyme found over-expressed in CRPC (62).

Similarly, metabolomics and lipidomic analysis demonstrated a significant impact of VPA/SIM treatment on metabolites functionally correlated with the modulated pathways reported above. For example, a clear downregulation of fatty acid and cholesterol was reported in PCa xenograft tumor tissues in VPA/SIM treated mice. In line with our data, Zhang et al., reported in rats orally treated with VPA, decreased levels of free fatty acids and the intermediate products of Krebs cycle such as arachidonic acid and citrate compared with the control group (63).

Moreover, in our analysis, we found in the VPA/SIM combination group, lower levels of glucose, but this effect was complemented by higher levels of enzymes involved in glycolysis and lower levels of ATP, final product of the glycolysis cues.

In accordance with our data a significant time- and concentration- dependent decrease in glucose levels in lymphoma and colon adenocarcinoma cell lines treated with statins was previously reported (64). Similarly, VPA treatment significantly resulted to decrease plasma glucose *in vivo* models (65). Also several clinical studies reported lower blood glucose levels in VPA-treated patients compared to controls (66). Finally, high levels of sarcosine, downmodulated by VPA/SIM, were found in sera of high grade compared to low grade PCa patients (67) as well as in urine samples of PCa patients in progression (68), being considered as a marker PCa aggressiveness (69)

Again, it is of note that recent findings have implicated YAP in the context of cell metabolism establishing that YAP/TAZ activity is affected by various metabolic cues, such as glucose, lipids, and metabolites, suggesting an emerging node in coordinating nutrient availability with cell growth and tissue homeostasis (70). For example, changes of nutrient and oxygen during metastasis may change YAP/TAZ binding partners and coordinate the cancer progression and metastasis (71). Here we also demonstrated the VPA/SIM-induced upregulation of AMPK, a key cellular energy sensor and a master regulator of cellular metabolism, that directly phosphorylates YAP at multiple sites to impair its activity, as previously demonstrated also by our group (5).

5. Conclusions

Altogether, we can suggest that VPA and SIM co-treatment inhibit tumor growth and progression influencing negatively the cancer cells cytoskeleton reorganization and the ECM by a complex mechanism involving multiple proteins regulation through inhibition of YAP/TAZ function. We also showed that VPA/SIM combination is able to target tumor cells metabolic reprogramming, by a mechanism involving modulation of specific enzyme expression, an effect again potentially linked to YAP signalling, confirming its central role in PCa tumorigenesis and as VPA/SIM main target. This study

significantly expands our understanding of the molecular mechanisms of the combination of these two safe and generic drug, contributing to the identification of potential biomarkers for patients' selection that can benefit from this treatment schedule. Indeed this finding corroborate the results obtained previously by our group on the repurposing of VPA and SIM combination in cancer treatment, an approach that beyond PCa could be extended to different cancer types in combination with other anticancer drugs and that deserve clinical evaluation.

Abbreviations

1H-NMR, Proton Nuclear Magnetic Resonance; ACON, Aconitase; ADT, Androgen deprivation therapy; ALDOA, Fructose-bisphosphate aldolase A; AMPK, AMP-activated protein kinase; ANKH1, Ankyrin repeat and KH domain-containing protein 1; AR, Androgen Receptor; ASGL1, Asparaginase; ATP, Adenosine triphosphate; CAN1, Calpain-1 catalytic subunit; CAN2, Calpain-2 catalytic subunit; CISY, Citrate synthase; CPNS1, Calpain small subunit; CSCs, Cancer stem cells;

CTGF, Connective tissue growth factor; CycD1, Cyclin D1; DFS, Disease-free survival; ECHD2, Enoyl-CoA hydratase; ECM, Extracellular matrix; ELN, Elastin; ENOA, Alpha-enolase; FDR, False discovery rate; G6PI, Glucose-6-phosphate isomerase; GO, Gene Ontology; GO:BP, GO biological process; GO:CC, GO cellular component; GO:MF, GO molecular function; HCD2, 3-hydroxyacyl-CoA dehydrogenase type-2; HDACi, Histone deacetylases inhibitors; HMGCR, HMG-CoA reductase; IPA, Ingenuity Pathway Analysis; KEGG, Kyoto Encyclopedia of Genes and Genomes; LAMC1, Laminin subunit gamma-1; LATS1, Large Tumor Suppressor Kinase 1; LBD, Ligand-binding domain; LC-MS/MS, Liquid chromatography-tandem mass spectrometry; mCRPC, Castration-resistant metastatic prostate cancer; MDH1, Cytosolic mitochondrial malate dehydrogenases; MDH2, Mitochondrial malate dehydrogenases; MMP1, Matrix metalloproteinase 1; MMP10, Matrix metalloproteinase 10; MST1/2, Mammalian Ste20-like kinases 1/2; MTAP2, Microtubule-associated protein 2; MVP, Mevalonate pathway; OS, Overall survival; PCA, Principal component plot; PCa, Prostate cancer; PCC, Pearson correlation coefficients; PLS-DA, Partial least squares-discriminant analysis; POSTN, Periostin; PSA, prostate-specific antigen; PTPRM, Protein-tyrosine phosphatase mu; RB11A, Ras-related protein Rab-11A; SDHA, Mitochondrial succinate dehydrogenase; SIM, Simvastatin; TAZ, Transcriptional coactivator with PDZ-binding motif; TCA, Tricarboxyloic acid cycle; TEAD, TEA domain; TGF-β, Transforming growth factor-beta; ULK1, Unc-51-like kinase 1; VPA, Valproic Acid; WP, WikiPathways; YAP, Yes-associated protein.

Declarations

Ethical Approval is not applicable.

Availability of data and materials

Proteomics and metabolomics raw data are available at https://zenodo.org/records/10118913

Conflict of interest

The authors declare no conflict of interest.

Founding

This work was supported by Italian Ministry of Health, Ricerca Corrente Funds to Istituto Nazionale Tumori G. Pascale project: Linea 2/2 to AB; and by Regione Campania grants: POR FESR 2014/2020 Progetto Campania Onco-Terapie/CUP: B61G18000470007; POR FESR 2014/2020 del progetto “PREMIO - Infrastruttura Per La Medicina Di Precisione In Oncologia”/CUP: B61C17000080007; POR FESR 2014 – 2020, del progetto “CIRO - Campania Imaging Infrastructure for Research in Oncology”/CUP: B61G17000190007.

Author contributions

FI, RL, BP, FB, AB were involved in conceptualization;

AB was responsible for project funding.

FI, RL and MSR were involved in in vivo models, collected and processed tumor samples.

FI and LA performed the data validation experiments.

RL, BP performed the proteomic experiments and initial data processing.

RL, FI, BP performed analysis of the proteomics data.

SC performed Metabolomics and Lipidomics experiments and analysis.

FI, RL, BP, EDG and AB wrote the manuscript with input from all co-authors.

References

1. Rawla P. Epidemiology of Prostate Cancer. World J Oncol. 2019;10(2):63-89.
2. Jang A, Sartor O, Barata PC, Paller CJ. Therapeutic Potential of PARP Inhibitors in the Treatment of Metastatic Castration-Resistant Prostate Cancer. Cancers (Basel). 2020;12(11).
3. Mehtala J, Zong J, Vassilev Z, Brobert G, Gabarro MS, Stattin P, et al. Overall survival and second primary malignancies in men with metastatic prostate cancer. PLoS One. 2020;15(2):e0227552.
4. Rizzo M. Mechanisms of docetaxel resistance in prostate cancer: The key role played by miRNAs. Biochim Biophys Acta Rev Cancer. 2021;1875(1):188481.
5. Iannelli F, Roca MS, Lombardi R, Ciardiello C, Grumetti L, De Rienzo S, et al. Synergistic antitumor interaction of valproic acid and simvastatin sensitizes prostate cancer to docetaxel by targeting CSCs compartment via YAP inhibition. J Exp Clin Cancer Res. 2020;39(1):213.
6. Ashburn TT, Thor KB. Drug repositioning: identifying and developing new uses for existing drugs. Nat Rev Drug Discov. 2004;3(8):673-83.

7. Salem O, Hansen CG. The Hippo Pathway in Prostate Cancer. Cells. 2019;8(4).
8. Liu X, Chinello C, Musante L, Cazzaniga M, Tataruch D, Calzaferri G, et al. Intraluminal proteome and peptidome of human urinary extracellular vesicles. Proteomics Clin Appl. 2015;9(5-6):568-73.
9. Silva JC, Gorenstein MV, Li GZ, Vissers JP, Geromanos SJ. Absolute quantification of proteins by LCMSE: a virtue of parallel MS acquisition. Mol Cell Proteomics. 2006;5(1):144-56.
10. Tyanova S, Temu T, Sinitcyn P, Carlson A, Hein MY, Geiger T, et al. The Perseus computational platform for comprehensive analysis of (prote)omics data. Nat Methods. 2016;13(9):731-40.
11. Lombardi R, Sonego M, Pucci B, Addi L, Iannelli F, Capone F, et al. HSP90 identified by a proteomic approach as druggable target to reverse platinum resistance in ovarian cancer. Mol Oncol. 2021;15(4):1005-23.
12. Huang da W, Sherman BT, Lempicki RA. Systematic and integrative analysis of large gene lists using DAVID bioinformatics resources. Nat Protoc. 2009;4(1):44-57.
13. Raudvere U, Kolberg L, Kuzmin I, Arak T, Adler P, Peterson H, et al. g:Profiler: a web server for functional enrichment analysis and conversions of gene lists (2019 update). Nucleic Acids Res. 2019;47(W1):W191-W8.
14. Pang Z, Chong J, Zhou G, de Lima Morais DA, Chang L, Barrette M, et al. MetaboAnalyst 5.0: narrowing the gap between raw spectra and functional insights. Nucleic Acids Res. 2021;49(W1):W388-W96.
15. Liu T, Mendes DE, Berkman CE. Prolonged androgen deprivation leads to overexpression of calpain 2: implications for prostate cancer progression. Int J Oncol. 2014;44(2):467-72.
16. Li J, Xu X, Jiang Y, Hansbro NG, Hansbro PM, Xu J, et al. Elastin is a key factor of tumor development in colorectal cancer. BMC Cancer. 2020;20(1):217.
17. Gong Y, Chippada-Venkata UD, Oh WK. Roles of matrix metalloproteinases and their natural inhibitors in prostate cancer progression. Cancers (Basel). 2014;6(3):1298-327.
18. Zhang G, Miyake M, Lawton A, Goodison S, Rosser CJ. Matrix metalloproteinase-10 promotes tumor progression through regulation of angiogenic and apoptotic pathways in cervical tumors. BMC Cancer. 2014;14:310.
19. Ozden F, Saygin C, Uzunaslan D, Onal B, Durak H, Aki H. Expression of MMP-1, MMP-9 and TIMP-2 in prostate carcinoma and their influence on prognosis and survival. J Cancer Res Clin Oncol. 2013;139(8):1373-82.
20. Zhang Y, Xi S, Chen J, Zhou D, Gao H, Zhou Z, et al. Overexpression of LAMC1 predicts poor prognosis and enhances tumor cell invasion and migration in hepatocellular carcinoma. J Cancer. 2017;8(15):2992-3000.
21. Cattrini C, Barboro P, Rubagotti A, Zinoli L, Zanardi E, Capaia M, et al. Integrative Analysis of Periostin in Primary and Advanced Prostate Cancer. Transl Oncol. 2020;13(7):100789.
22. Hu Q, Tong S, Zhao X, Ding W, Gou Y, Xu K, et al. Periostin Mediates TGF-beta-Induced Epithelial Mesenchymal Transition in Prostate Cancer Cells. Cell Physiol Biochem. 2015;36(2):799-809.

23. Dong Q, Fu L, Zhao Y, Du Y, Li Q, Qiu X, et al. Rab11a promotes proliferation and invasion through regulation of YAP in non-small cell lung cancer. Oncotarget. 2017;8(17):27800-11.
24. Dupont S, Morsut L, Aragona M, Enzo E, Giulitti S, Cordenonsi M, et al. Role of YAP/TAZ in mechanotransduction. Nature. 2011;474(7350):179-83.
25. Costello LC, Franklin RB. The clinical relevance of the metabolism of prostate cancer; zinc and tumor suppression: connecting the dots. Mol Cancer. 2006;5:17.
26. Fabregat A, Sidiropoulos K, Viteri G, Forner O, Marin-Garcia P, Arnau V, et al. Reactome pathway analysis: a high-performance in-memory approach. BMC Bioinformatics. 2017;18(1):142.
27. You X, Tian J, Zhang H, Guo Y, Yang J, Zhu C, et al. Loss of mitochondrial aconitase promotes colorectal cancer progression via SCD1-mediated lipid remodeling. Mol Metab. 2021;48:101203.
28. Sajnani K, Islam F, Smith RA, Gopalan V, Lam AK. Genetic alterations in Krebs cycle and its impact on cancer pathogenesis. Biochimie. 2017;135:164-72.
29. Leandro JG, Espindola-Netto JM, Vianna MC, Gomez LS, DeMaria TM, Marinho-Carvalho MM, et al. Exogenous citrate impairs glucose tolerance and promotes visceral adipose tissue inflammation in mice. Br J Nutr. 2016;115(6):967-73.
30. Silva MF, Aires CC, Luis PB, Ruiter JP, L IJ, Duran M, et al. Valproic acid metabolism and its effects on mitochondrial fatty acid oxidation: a review. J Inherit Metab Dis. 2008;31(2):205-16.
31. Lu M, Zhan X. The crucial role of multiomic approach in cancer research and clinically relevant outcomes. EPMA J. 2018;9(1):77-102.
32. Moya IM, Halder G. Hippo-YAP/TAZ signalling in organ regeneration and regenerative medicine. Nat Rev Mol Cell Biol. 2019;20(4):211-26.
33. Chen YA, Lu CY, Cheng TY, Pan SH, Chen HF, Chang NS. WW Domain-Containing Proteins YAP and TAZ in the Hippo Pathway as Key Regulators in Stemness Maintenance, Tissue Homeostasis, and Tumorigenesis. Front Oncol. 2019;9:60.
34. Santos DM, Pantano L, Pronzati G, Grasberger P, Probst CK, Black KE, et al. Screening for YAP Inhibitors Identifies Statins as Modulators of Fibrosis. Am J Respir Cell Mol Biol. 2020;62(4):479-92.
35. Hao F, Xu Q, Wang J, Yu S, Chang HH, Sinnett-Smith J, et al. Lipophilic statins inhibit YAP nuclear localization, co-activator activity and colony formation in pancreatic cancer cells and prevent the initial stages of pancreatic ductal adenocarcinoma in KrasG12D mice. PLoS One. 2019;14(5):e0216603.
36. Koohestanimobarhan S, Salami S, Imeni V, Mohammadi Z, Bayat O. Lipophilic statins antagonistically alter the major epithelial-to-mesenchymal transition signaling pathways in breast cancer stem-like cells via inhibition of the mevalonate pathway. J Cell Biochem. 2019;120(2):2515-31.
37. Mi W, Lin Q, Childress C, Sudol M, Robishaw J, Berlot CH, et al. Geranylgeranylation signals to the Hippo pathway for breast cancer cell proliferation and migration. Oncogene. 2015;34(24):3095-106.

38. Huang J, Zhang L, Wan D, Zhou L, Zheng S, Lin S, et al. Extracellular matrix and its therapeutic potential for cancer treatment. Signal Transduct Target Ther. 2021;6(1):153.
39. Jang HS, Lal S, Greenwood JA. Calpain 2 is required for glioblastoma cell invasion: regulation of matrix metalloproteinase 2. Neurochem Res. 2010;35(11):1796-804.
40. Jorfi S, Ansa-Addo EA, Kholia S, Stratton D, Valley S, Lange S, et al. Inhibition of microvesiculation sensitizes prostate cancer cells to chemotherapy and reduces docetaxel dose required to limit tumor growth in vivo. Sci Rep. 2015;5:13006.
41. Bhat KM, Setaluri V. Microtubule-associated proteins as targets in cancer chemotherapy. Clin Cancer Res. 2007;13(10):2849-54.
42. Lin C, Blessing AM, Pulliam TL, Shi Y, Wilkenfeld SR, Han JJ, et al. Inhibition of CAMKK2 impairs autophagy and castration-resistant prostate cancer via suppression of AMPK-ULK1 signaling. Oncogene. 2021;40(9):1690-705.
43. Sorrentino G, Ruggeri N, Zannini A, Ingallina E, Bertolio R, Marotta C, et al. Glucocorticoid receptor signalling activates YAP in breast cancer. Nat Commun. 2017;8:14073.
44. Li Y, Wang J, Zhong W. Regulation and mechanism of YAP/TAZ in the mechanical microenvironment of stem cells (Review). Mol Med Rep. 2021;24(1).
45. Zanconato F, Cordenonsi M, Piccolo S. YAP and TAZ: a signalling hub of the tumour microenvironment. Nat Rev Cancer. 2019;19(8):454-64.
46. Shi X, Young CD, Zhou H, Wang X. Transforming Growth Factor-beta Signaling in Fibrotic Diseases and Cancer-Associated Fibroblasts. Biomolecules. 2020;10(12).
47. Noguchi S, Saito A, Nagase T. YAP/TAZ Signaling as a Molecular Link between Fibrosis and Cancer. Int J Mol Sci. 2018;19(11).
48. Wu F, Yang J, Liu J, Wang Y, Mu J, Zeng Q, et al. Signaling pathways in cancer-associated fibroblasts and targeted therapy for cancer. Signal Transduct Target Ther. 2021;6(1):218.
49. Liu P, Zhang C, Liao Y, Liu J, Huang J, Xia M, et al. High expression of PTPRM predicts poor prognosis and promotes tumor growth and lymph node metastasis in cervical cancer. Cell Death Dis. 2020;11(8):687.
50. Vallianou NG, Kostantinou A, Kougias M, Kazazis C. Statins and cancer. Anticancer Agents Med Chem. 2014;14(5):706-12.
51. Frick M, Dulak J, Cisowski J, Jozkowicz A, Zwick R, Alber H, et al. Statins differentially regulate vascular endothelial growth factor synthesis in endothelial and vascular smooth muscle cells. Atherosclerosis. 2003;170(2):229-36.
52. Tate R, Zona E, De Cicco R, Trotta V, Urciuoli M, Morelli A, et al. Simvastatin inhibits the expression of stemness-related genes and the metastatic invasion of human cancer cells via destruction of the cytoskeleton. Int J Oncol. 2017;51(6):1851-9.
53. Ellis L, Hammers H, Pili R. Targeting tumor angiogenesis with histone deacetylase inhibitors. Cancer Lett. 2009;280(2):145-53.

54. Eckschlager T, Plch J, Stiborova M, Hrabeta J. Histone Deacetylase Inhibitors as Anticancer Drugs. Int J Mol Sci. 2017;18(7).
55. Cai Z, Deng Y, Ye J, Zhuo Y, Liu Z, Liang Y, et al. Aberrant Expression of Citrate Synthase is Linked to Disease Progression and Clinical Outcome in Prostate Cancer. Cancer Manag Res. 2020;12:6149-63.
56. Abdel-Mawgoud AM, Lepine F, Deziel E. A chiral high-performance liquid chromatography-tandem mass spectrometry method for the stereospecific analysis of enoyl-coenzyme A hydratases/isomerases. J Chromatogr A. 2013;1306:37-43.
57. Zhang J, Ibrahim MM, Sun M, Tang J. Enoyl-coenzyme A hydratase in cancer. Clin Chim Acta. 2015;448:13-7.
58. Paiva H, Thelen KM, Van Coster R, Smet J, De Paepe B, Mattila KM, et al. High-dose statins and skeletal muscle metabolism in humans: a randomized, controlled trial. Clin Pharmacol Ther. 2005;78(1):60-8.
59. Salimi A, Gholamifar E, Naserzadeh P, Hosseini MJ, Pourahmad J. Toxicity of lithium on isolated heart mitochondria and cardiomyocyte: A justification for its cardiotoxic adverse effect. J Biochem Mol Toxicol. 2017;31(2).
60. Sciacovelli M, Frezza C. Oncometabolites: Unconventional triggers of oncogenic signalling cascades. Free Radic Biol Med. 2016;100:175-81.
61. Dalla Pozza E, Dando I, Pacchiana R, Liboi E, Scupoli MT, Donadelli M, et al. Regulation of succinate dehydrogenase and role of succinate in cancer. Semin Cell Dev Biol. 2020;98:4-14.
62. Sircar K, Huang H, Hu L, Cogdell D, Dhillon J, Tzelepi V, et al. Integrative molecular profiling reveals asparagine synthetase is a target in castration-resistant prostate cancer. Am J Pathol. 2012;180(3):895-903.
63. Zhang LF, Liu LS, Chu XM, Xie H, Cao LJ, Guo C, et al. Combined effects of a high-fat diet and chronic valproic acid treatment on hepatic steatosis and hepatotoxicity in rats. Acta Pharmacol Sin. 2014;35(3):363-72.
64. Malenda A, Skrobanska A, Issat T, Winiarska M, Bil J, Oleszczak B, et al. Statins impair glucose uptake in tumor cells. Neoplasia. 2012;14(4):311-23.
65. Khan S, Jena G. Valproic Acid Improves Glucose Homeostasis by Increasing Beta-Cell Proliferation, Function, and Reducing its Apoptosis through HDAC Inhibition in Juvenile Diabetic Rat. J Biochem Mol Toxicol. 2016;30(9):438-46.
66. Rakitin A. Does Valproic Acid Have Potential in the Treatment of Diabetes Mellitus? Front Endocrinol (Lausanne). 2017;8:147.
67. Kumar D, Gupta A, Mandhani A, Sankhwar SN. Metabolomics-derived prostate cancer biomarkers: fact or fiction? J Proteome Res. 2015;14(3):1455-64.
68. Jiang Y, Cheng X, Wang C, Ma Y. Quantitative determination of sarcosine and related compounds in urinary samples by liquid chromatography with tandem mass spectrometry. Anal Chem. 2010;82(21):9022-7.

69. Koutros S, Meyer TE, Fox SD, Issaq HJ, Veenstra TD, Huang WY, et al. Prospective evaluation of serum sarcosine and risk of prostate cancer in the Prostate, Lung, Colorectal and Ovarian Cancer Screening Trial. Carcinogenesis. 2013;34(10):2281-5.
70. Koo JH, Guan KL. Interplay between YAP/TAZ and Metabolism. Cell Metab. 2018;28(2):196-206.
71. Elisi GM, Santucci M, D'Arca D, Lauriola A, Marverti G, Losi L, et al. Repurposing of Drugs Targeting YAP-TEAD Functions. Cancers (Basel). 2018;10(9).

Figures

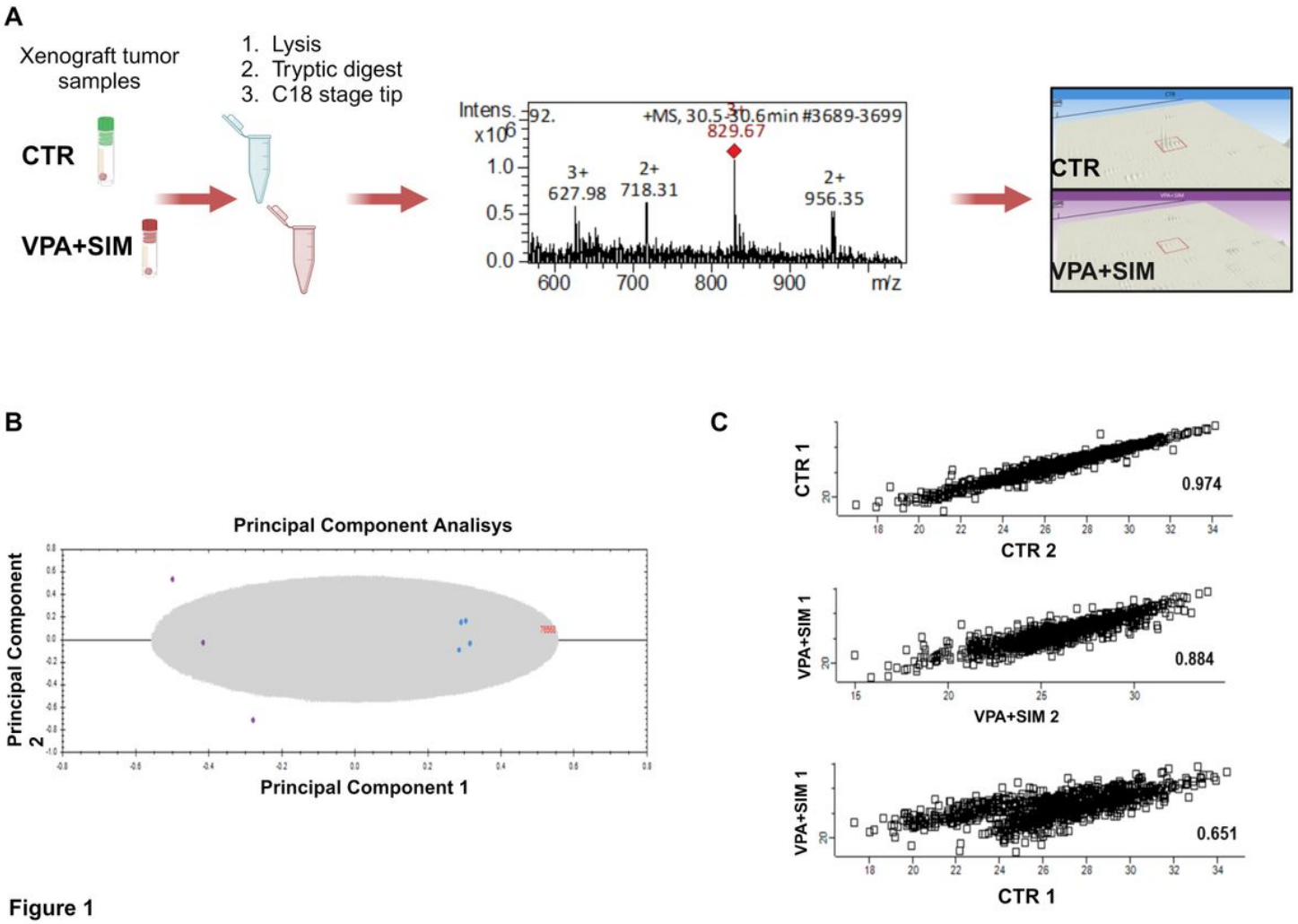

Figure 1

Figure 1

Schematic representation of workflow of label-free LC-MS MS-based protein quantification. **(A)** Digested peptides of 22Rv1 CTR and VPA/SIM treated group Xenograft tumor sample is shown. Resulting peptide profiles are aligned and their intensities are quantified as shown by 3D ion peak intensity view. **(B)**PCA plot unsupervised multivariate analysis on proteomic data of the proteomic approach where we showed the biological replicates of 22Rv1 CTR by light blue circles and treated 22Rv1 by purple circles. **(C)** Scatter

plot depicting the Pearson's correlation between the biological replicates. An absolute value of about 0.8-1 indicated a very good linear relationship. Figure created with BioRender.com

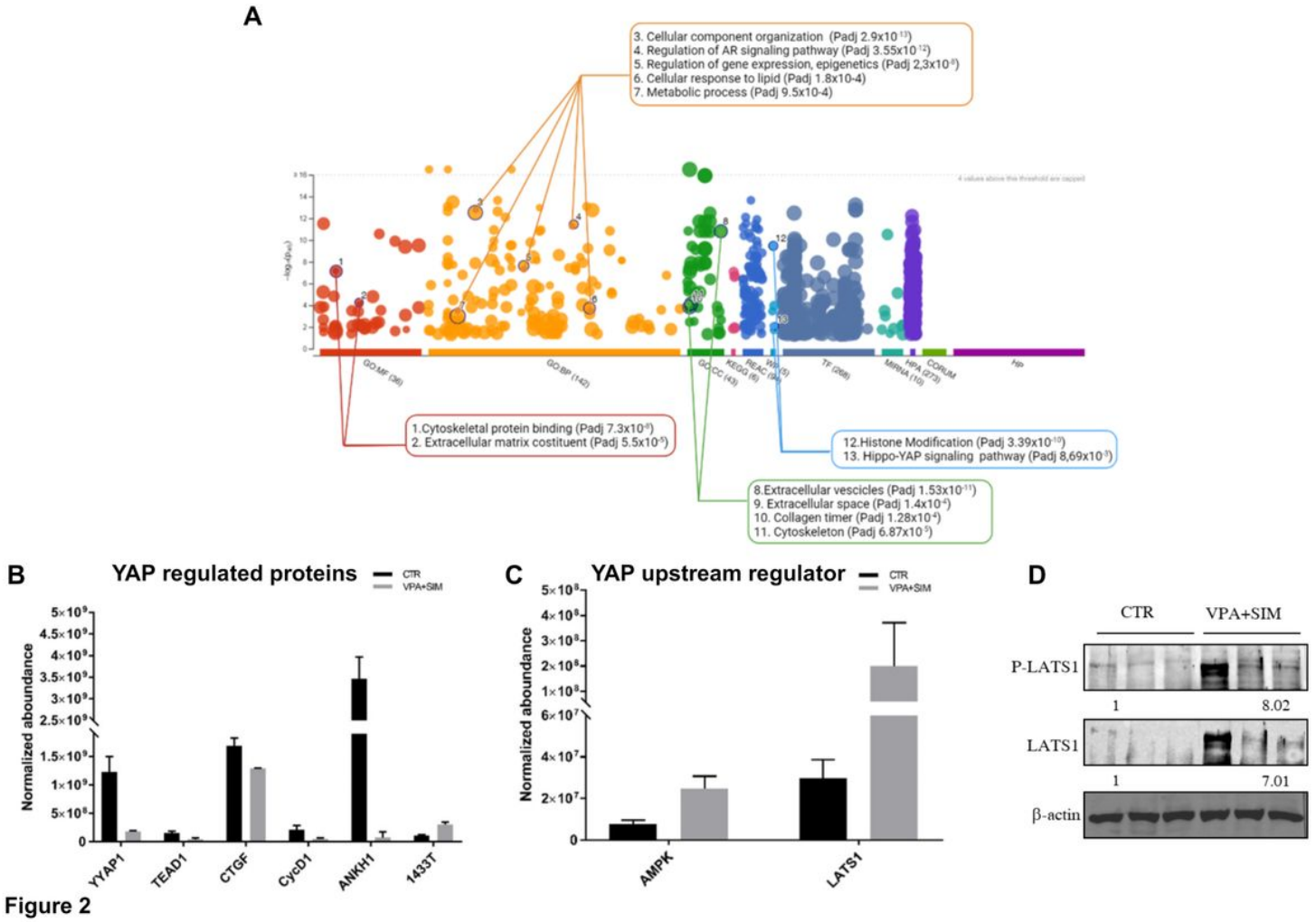

Figure 2

Figure 2

Functional enrichment analysis using g:Profiler software and western blot analysis. **(A)** The significantly changed terms enriched by GO and Wikipathways (WP). **(B-C)**Normalized abundance of YAP target genes and upstream regulators. The used values refer to Progenesis data (http://www.nonlinear.com/progenesis/ qi/) that quantified proteins based on peptide ion signal peak intensity. **(D)** Western blot analysis of phospho LATS1 (pLATS1) and LATS1 in lysates from three representative xenograft tumor samples from each treatment group and control. β-actin expression serves as loading control. Western blot quantification was performed by ImageJ software using the mean value of the three samples for each experimental group. Densitometric analysis was reported as ratio relative to the indicated loading control. Figure created with BioRender.com

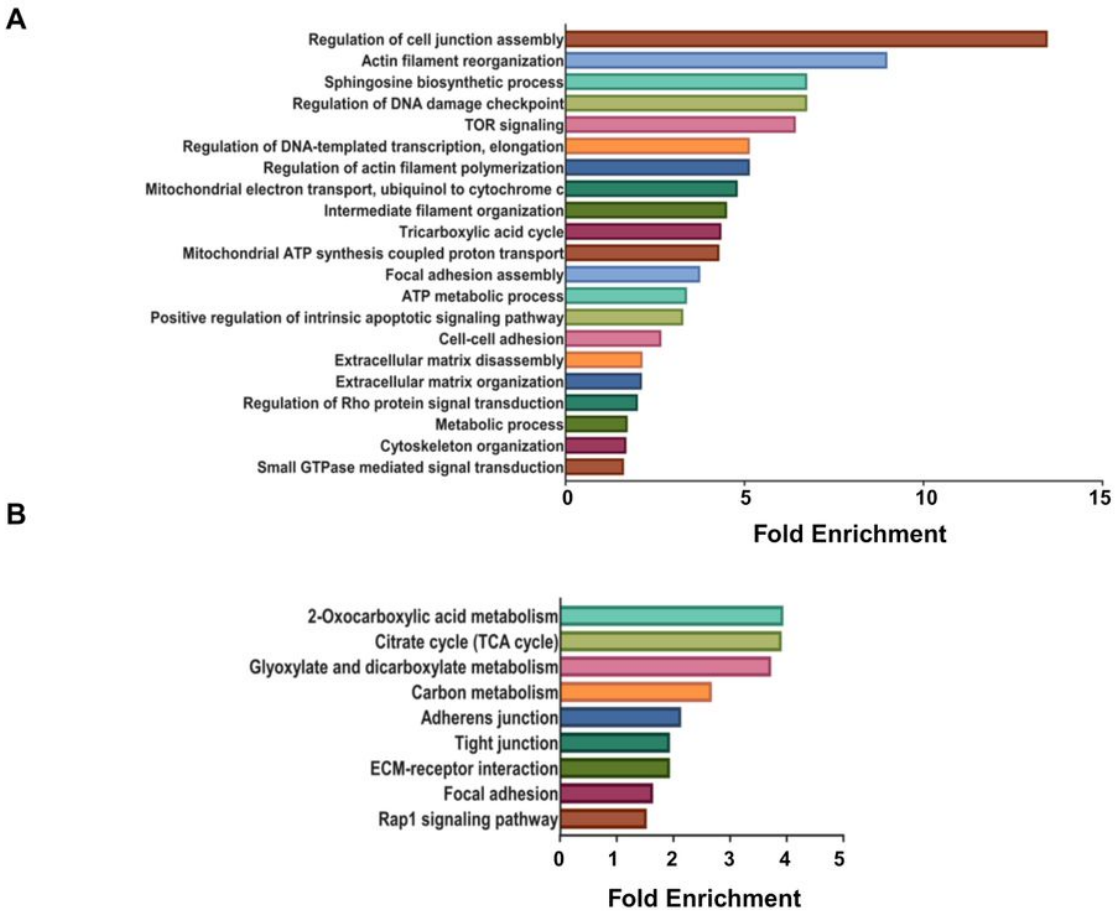

Figure 3

Figure 3

Functional enrichment analysis on the significant proteins using DAVID tool in terms of **(A)** Gene Ontology (GO) biological processes and **(B)** KEGG pathways. Figure created with BioRender.com

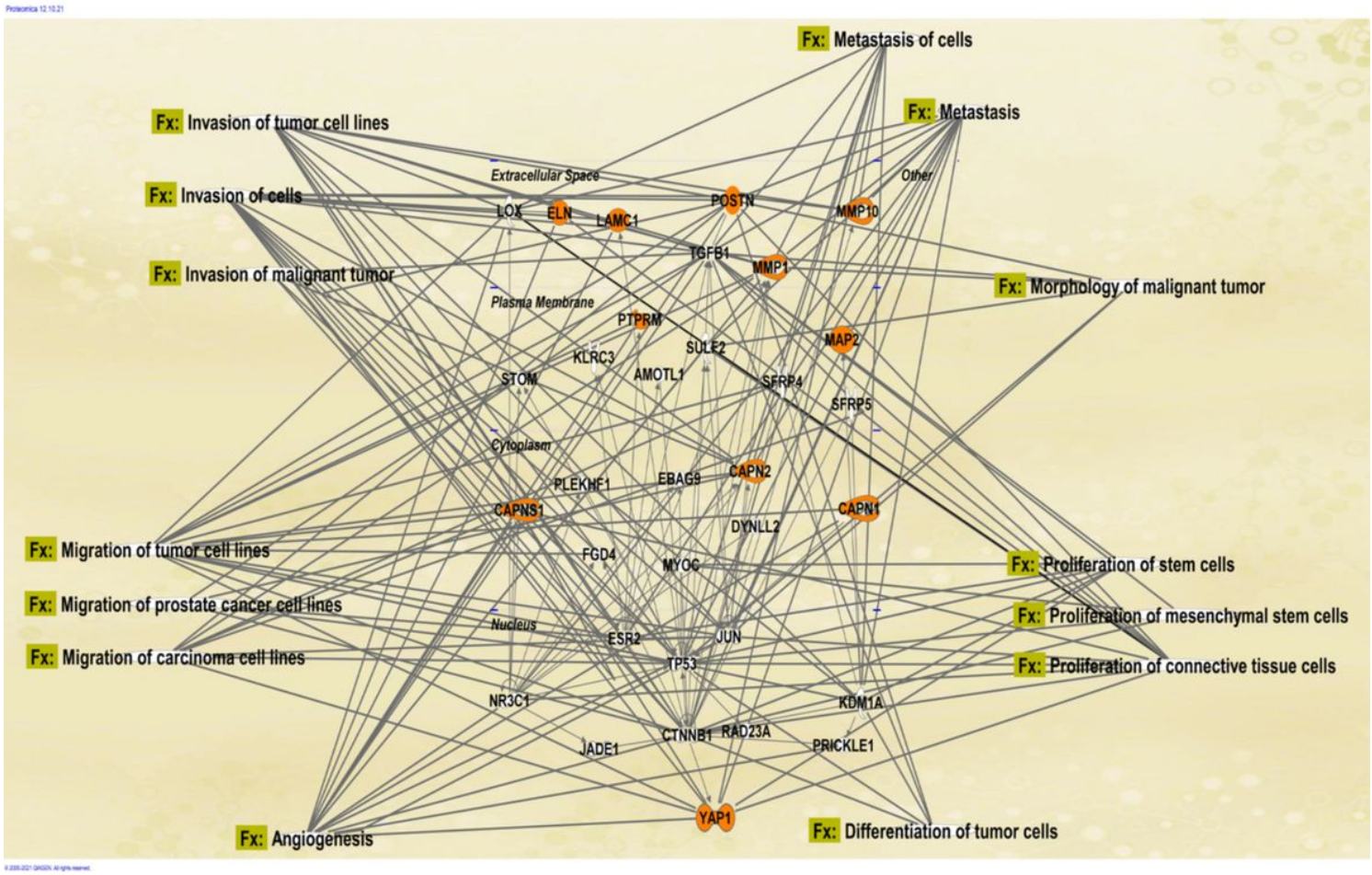

Figure 4

Figure 4

Visual representation of the network generated by IPA evidencing direct interactions including 11 out of 12 identified proteins (showed in orange). The molecular function (Fx) related to the proteins present in the network were reported. Figure created with BioRender.com

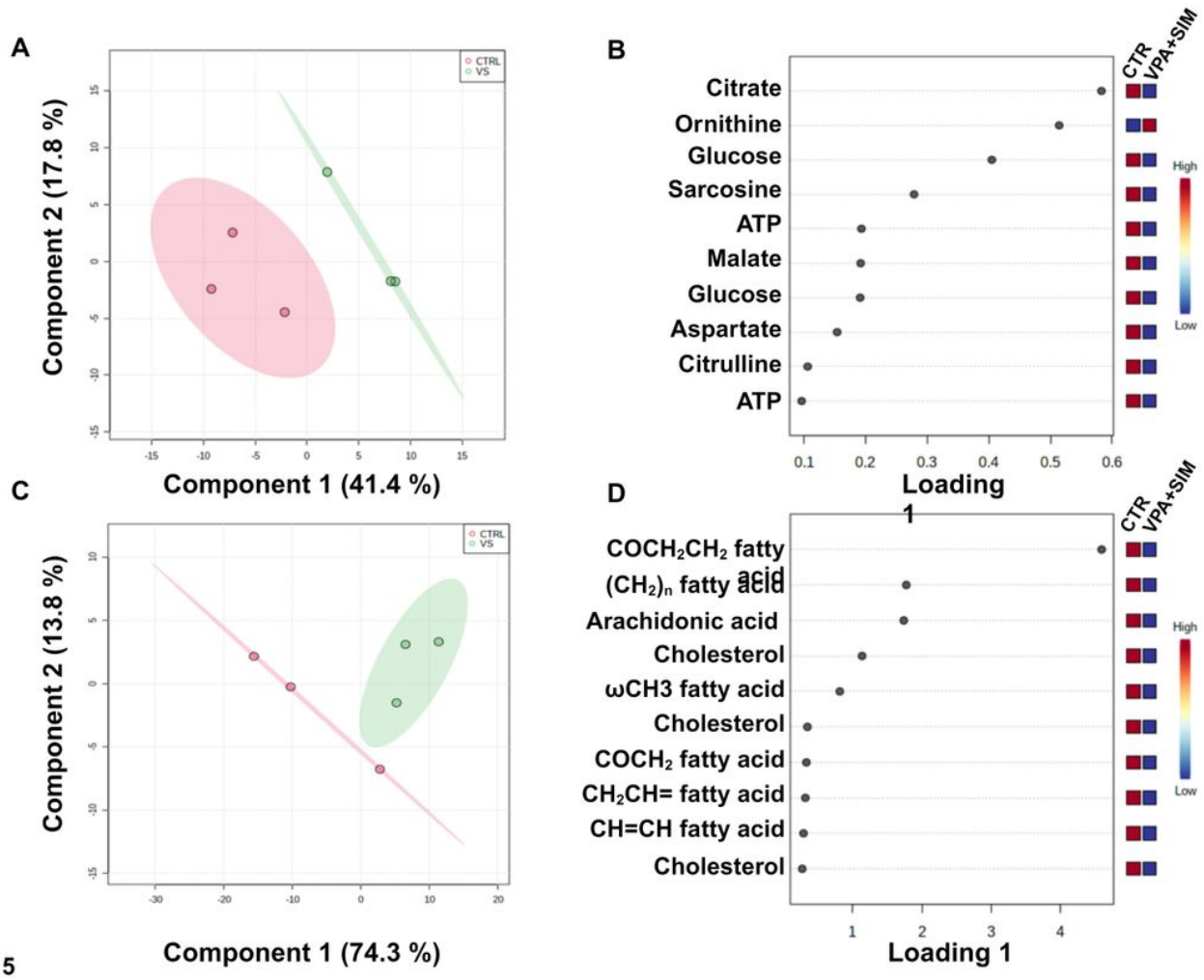

Figure 5

Figure 5

Score and Loading plots related to ^{1}H-NMR analysis of **(A, B)** polar and (**C, D**) lipidic fractions obtained comparing the spectra obtained for the 22Rv1 VPA/SIM treated vs CTR groups. The loading plots highlighted the top ten proton signals of metabolites/lipids that resulted significantly different between two analyzed groups. Figure created with BioRender.com

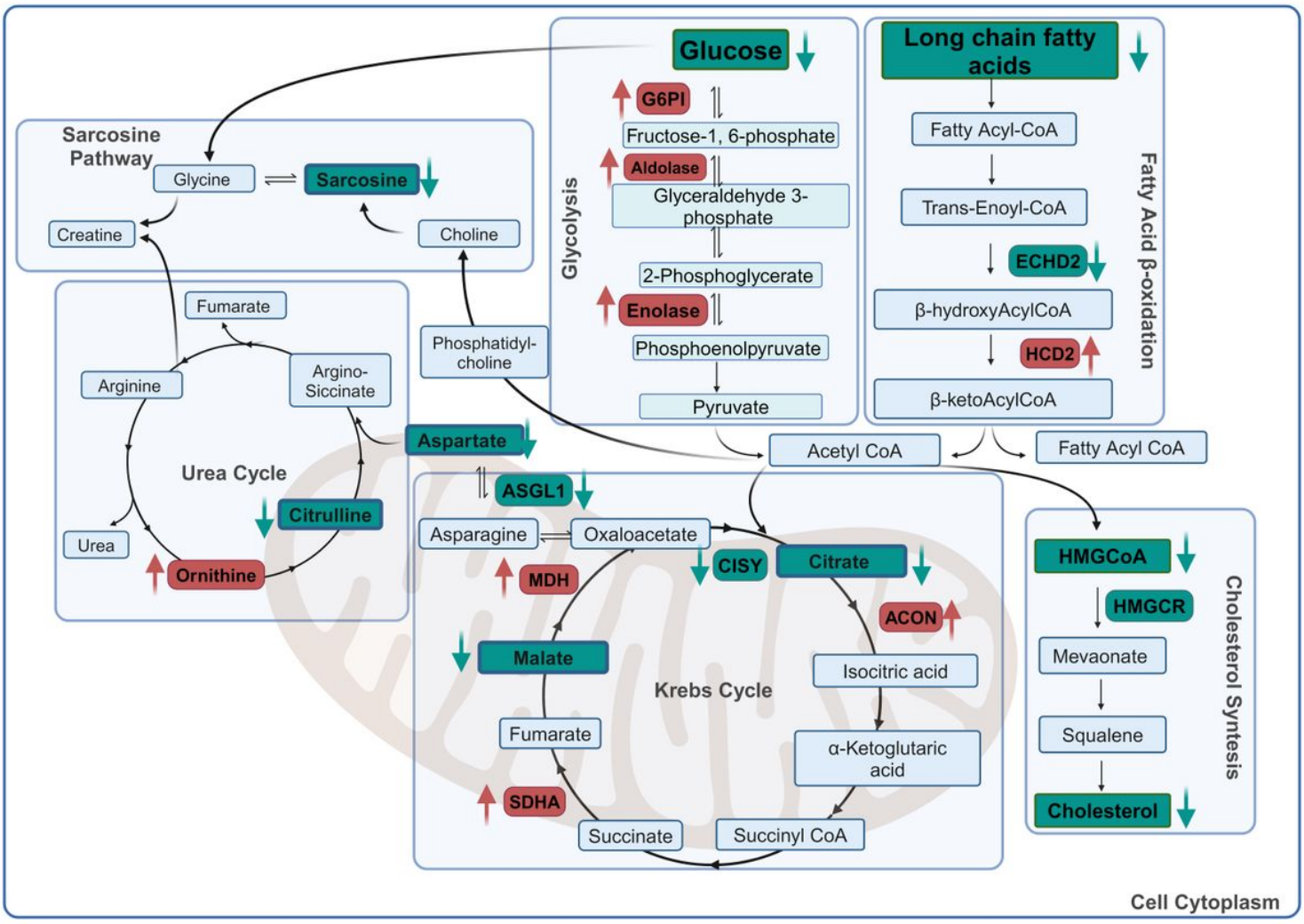

Figure 6

Figure 6

Schematic representation of the metabolic mechanisms modulated in the 22Rv1 VPA/SIM treated vs CTR groups. We highlighted the enzymes (red) and the metabolites (green) resulted to be increased and decreased in the 22Rv1 VPA/SIM treated group. Figure created with BioRender.com

Supplementary Files

This is a list of supplementary files associated with this preprint. Click to download.

- AdditionalFile1.pdf
- AdditionalFile2.xls
- AdditionalFile3.pdf